ACS Catalysis

Research Article

Cite This: ACS Catal. 2019, 9, 6407−6414

pubs.acs.org/acscatalysis

Mechanistic Basis for Effects of High-Pressure H_2 Cofeeds on Methanol-to-Hydrocarbons Catalysis over Zeolites

Sukaran S. Arora,[†,‡] Zhichen Shi,[†,‡] and Aditya Bhan*[,†]

[†]Department of Chemical Engineering and Materials Science, University of Minnesota, Minneapolis, Minnesota 55455, United States

Supporting Information

ABSTRACT: Cofeeding high-pressure (16 bar) H_2 with methanol (0.005 bar) during methanol-to-hydrocarbons conversion over acidic zeolites with varying topologies (CHA, AEI, FER, and BEA) results in a ∼2× to >15× enhancement in catalyst lifetime compared to He cofeeds, as determined by the cumulative turnovers attained per proton before the final methanol conversion level drops below 15%C. These beneficial effects of prolonged catalyst lifetime are observed without any impact on the carbon backbone of effluent hydrocarbon products characteristic of the particular zeolite topology. The olefins-to-paraffins ratio of C_{2+} hydrocarbons, however, decreases due to enhanced paraffins production, and the magnitude of this decrement depends on the specific zeolite topology. The observations of marked lifetime improvements and topology-dictated variations in the paraffin make of MTH effluent with H_2 cofeeds can be interpreted based on the different proclivities of zeolitic protons confined in varying topological environments for catalyzing hydrogenation of hydrocarbons that are predominantly formed via formaldehyde-based alkylation routes (e.g., 1,3-butadiene) or methanol-based alkylation routes (e.g., ethene and propene). Independent kinetic studies reveal that measured hydrogenation rates per H^+ of 1,3-butadiene are at least 1 order of magnitude (∼7× to ∼320×) higher than that of ethene or propene, which provides an explanation for the observed lifetime improvements in MTH with H_2 cofeeds. Further, trends in the reactivities of ethene and propene with H_2 over the different zeolites help explicate the topology-dependent variations in the paraffin content of the effluent hydrocarbons during MTH with H_2 cofeeds.

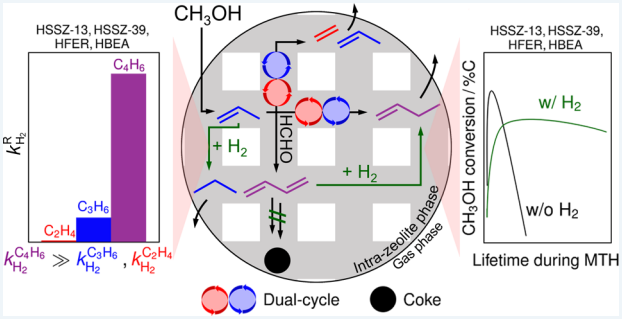

KEYWORDS: *methanol-to-hydrocarbons, alkene hydrogenation, kinetics, zeolites, lifetime, deactivation*

INTRODUCTION

The identity and distribution of hydrocarbon products in methanol-to-hydrocarbon (MTH) conversion primarily depend on the topological features of the zeolite used as the solid acid catalyst. The conversion of methanol over proton-form small-pore HSSZ-13 and HSSZ-39 zeolites characterized by large ellipsoidal cages interconnected via narrow 8-membered ring windows (3.8 Å × 3.8 Å)[1] results in the selective production of light hydrocarbons (C_2−C_4),[2−4] while proton-form medium-pore HFER and large-pore HBEA zeolites primarily yield gasoline-range hydrocarbons—C_{4+} and aromatics.[5−7] The mechanistic origins of these hydrocarbon products are rationalized based on the hydrocarbon pool mechanism which can be described by a dual-cycle schematic that considers olefins and aromatics, interconvertible via chemistries of dehydrocyclization and dealkylation, as cocatalytic centers involved in distinct propagation events based on methylation and β-scission of olefins (referred as the "olefins cycle") and methylation and dealkylation of aromatics (referred as the "aromatics cycle").[5,8−12] The aforementioned differences in the identity and distribution of hydrocarbon products depending on the zeolite topology are a consequence of the relative propagation of the olefins and aromatics cycles. The small-pore zeolites, HSSZ-13 and HSSZ-39, preferentially propagate the aromatics cycle in the large cages while only allowing the effusion of light hydrocarbons (C_2− C_4); on the other hand, medium- and large-pore zeolites, HFER and HBEA, allow the simultaneous propagation of the olefins and aromatics cycles and the effusion of both larger C_{4+} hydrocarbons and aromatics. The propagation events in MTH, however, terminate with reaction progress due to the transformation of active olefin and aromatic species to inactive polycyclics, thereby causing catalyst deactivation.[5,7,13,14] The formation of formaldehyde in transfer dehydrogenation events involving methanol and its involvement in electrophilic addition reactions with olefins resulting in polyenes that can undergo dehydrocyclization to form aromatics and in electrophilic substitution reactions with aromatics to form intermediates that can further transform to polycyclic compounds has been documented in the recent literature.[15−22]

Received: March 5, 2019
Revised: May 24, 2019
Published: May 30, 2019

DOI: 10.1021/acscatal.9b00969
ACS Catal. 2019, 9, 6407−6414

Table 1. Physical and Chemical Characteristics of Zeolites Used in the Study

zeolite	framework type	source	Si/Al[a]	H^+ density (mmol g^{-1})	surface area BET (m^2 g^{-1})	surface area Langmuir (m^2 g^{-1})	micropore volume (cm^3 g^{-1})
HSSZ-13	CHA	ACS material	13.2	0.44	560	825	0.28
HSSZ-39	AEI	ACS material	9.0	0.83	506	761	0.27
HFER	FER	Zeolyst	10.0	0.64	283	419	0.13
HBEA	BEA	Zeolyst	12.4	0.33	530	798	0.16

[a]Obtained from energy dispersive X-ray spectroscopy (EDS) measurements.

Arora et al.[23] recently reported that cofeeding high-pressure H_2 results in the interception of formaldehyde-mediated alkylation pathways thereby resulting in longer catalyst lifetimes during MTH over HSAPO-34. Here, we demonstrate the utility of this strategy of cofeeding high-pressure H_2 for improving the MTH lifetime of various zeolites with distinct topologies (CHA, AEI, FER, and BEA). Besides the effect on lifetime, cofeeding H_2 also results in enhanced formation of paraffins, which manifests in lower olefins-to-paraffins ratios of the effluent hydrocarbons compared to the case of He cofeeds, albeit to varying extents depending on the specific zeolite topology. We provide a mechanistic basis for these observations in context of the reactivity of H_2 with 1,3-butadiene (formed via reaction between formaldehyde and propene[20,22,24,25]) that intercepts its transformation to inactive polycyclics compared to the reactivity of H_2 with ethene and propene (formed from methanol-based alkylation routes) that results in the formation of undesired paraffins in MTH over zeolites. This reactivity is quantified by hydrogenation rate constants measured during reactions of ethene, propene, and 1,3-butadiene with H_2 over the different zeolites in independent kinetic studies reported herein.

MATERIALS AND METHODS

Catalyst Characterization. The small-pore zeolites, SSZ-13 and SSZ-39, were obtained from ACS Material while the medium- and large-pore zeolites, FER and BEA, were sourced from Zeolyst (CP914C and CP814E, respectively) in their ammonium-form and converted to the proton-form by thermal treatment in flowing dry air (1.67 cm^3 s^{-1}; Zero grade, Matheson) at 823 K (0.0167 K s^{-1} ramp rate from RT) for 4 h followed by pelletization, crushing, and sieving to retain 180−250 μm (60−80 mesh) aggregates. The Brønsted acid site densities of these samples are listed in Table 1 and were obtained from NH_3 temperature-programmed desorption (TPD) measurements performed by saturating ∼50 mg of the proton-form samples with flowing 500 ppm of NH_3 (1.67 cm^3 s^{-1}; 1.01% in balance helium, Certified Standard, Praxair) at 423 K followed by a purge in flowing helium (1.67 cm^3 s^{-1}; 99.9999%, Matheson) for 4 h at 423 K to desorb any physisorbed NH_3, and ramping the temperature at 0.167 K s^{-1} ramp rate to 823 K during which the effluent stream was monitored via mass spectrometry (MKS Cirrus) for signals corresponding to m/z = 16 (for NH_3) and 40 (for Ar [0.083 cm^3 s^{-1}; 99.9999%, Matheson] used as the internal standard; Figure S1a). Further, the Brønsted acid site count was also ascertained for the HFER and HBEA samples by pyridine IR measurements (Table S1 and Figure S1b) performed on self-supporting wafers following a procedure similar to the one reported by Harris et al.[26] The integrated molar extinction coefficient (IMEC) for the IR band at 1542 cm^{-1} assigned to pyridine adsorbed on Brønsted acid sites was taken as 1.13.[27] These measurements were not performed on the small-pore zeolite (HSSZ-13 and HSSZ-39) samples since pyridine is too bulky to enter the pores of these zeolites. The Brønsted acid site densities thus obtained are tabulated in Table S1 along with the corresponding values enumerated from NH_3-TPD, and are within a factor of ∼0.8−1 of the NH_3-TPD count. To be consistent, all rate constants reported herein are obtained after normalization of the observed rates by the site count measured from NH_3-TPD. X-ray diffraction patterns were collected using a Bruker microdiffractometer with Cu Kα (λ = 1.54 Å) as the radiation source to confirm the framework type of the respective samples and are shown in Figure S2. The t-plot micropore volume, Brunauer−Emmett−Teller (BET), and Langmuir surface areas of the samples are listed in Table 1 and were obtained from N_2 adsorption measurements collected at 77 K using ASAP 2020 (Micromeritics). The samples were degassed by evacuating the sample tube to ≤10 μmHg at 363 K (0.083 K s^{-1} ramp rate from RT) followed by thermal treatment in vacuo at 723 K (0.083 K s^{-1} ramp rate from 363 K) for 4 h prior to N_2 adsorption.

Catalytic Testing. All experiments were performed in a tubular glass-lined stainless steel reactor (6.35 mm O.D. and 4 mm I.D., SGE Analytical Science). The proton-form zeolite aggregates were physically mixed with aggregates of sand (subjected prior to an overnight wash in 2 M HNO_3 solution followed by DI water rinse until pH ∼7, and a final thermal treatment in flowing dry air (1.67 cm^3 s^{-1}) at 1273 K (0.083 K s^{-1} ramp rate from RT) for 16 h; 10 < $wt_{diluent}/wt_{cat}$ < 15) and packed in the middle of the reactor tube between quartz wool (Technical Glass Products) plugs. The tubular reactor was then placed inside a resistively heated furnace (Applied Test Systems); the reaction temperature was measured using a K-type thermocouple (Omega) wrapped around the reactor periphery with the tip placed at the center of the catalyst bed and regulated with an electronic controller (Watlow). The free volume above and below the catalyst bed was filled by quartz rods (3 mm O.D.; Technical Glass Products) to prevent any vertical displacement of the catalyst bed. Prior to catalytic measurements, the catalyst bed was pretreated in flowing dry air (1.67 cm^3 s^{-1}) at 823 K (0.0167 K s^{-1} ramp rate from RT) for 4 h prior to cooling down to the desired reaction temperature in helium flow (1.67 cm^3 s^{-1}). The gas-phase pressure of the influent and effluent streams was measured using pressure transducers (Omega) placed upstream and downstream of the reactor tube. The composition of the reactant and product streams were quantified using a gas chromatograph (Agilent GC 7890A) equipped with a dimethylpolysiloxane HP-1 column (50 m × 320 μm × 0.52 μm) connected to a flame ionization detector for detection of hydrocarbons and oxygenates, and a GS-GasPro column (60 m × 320 μm) or Porapak Q (4.6 m × 3.2 mm × 2 mm) connected to a thermal conductivity detector for detecting permanent gases (H_2, Ar, and N_2).

DOI: 10.1021/acscatal.9b00969
ACS Catal. 2019, 9, 6407−6414

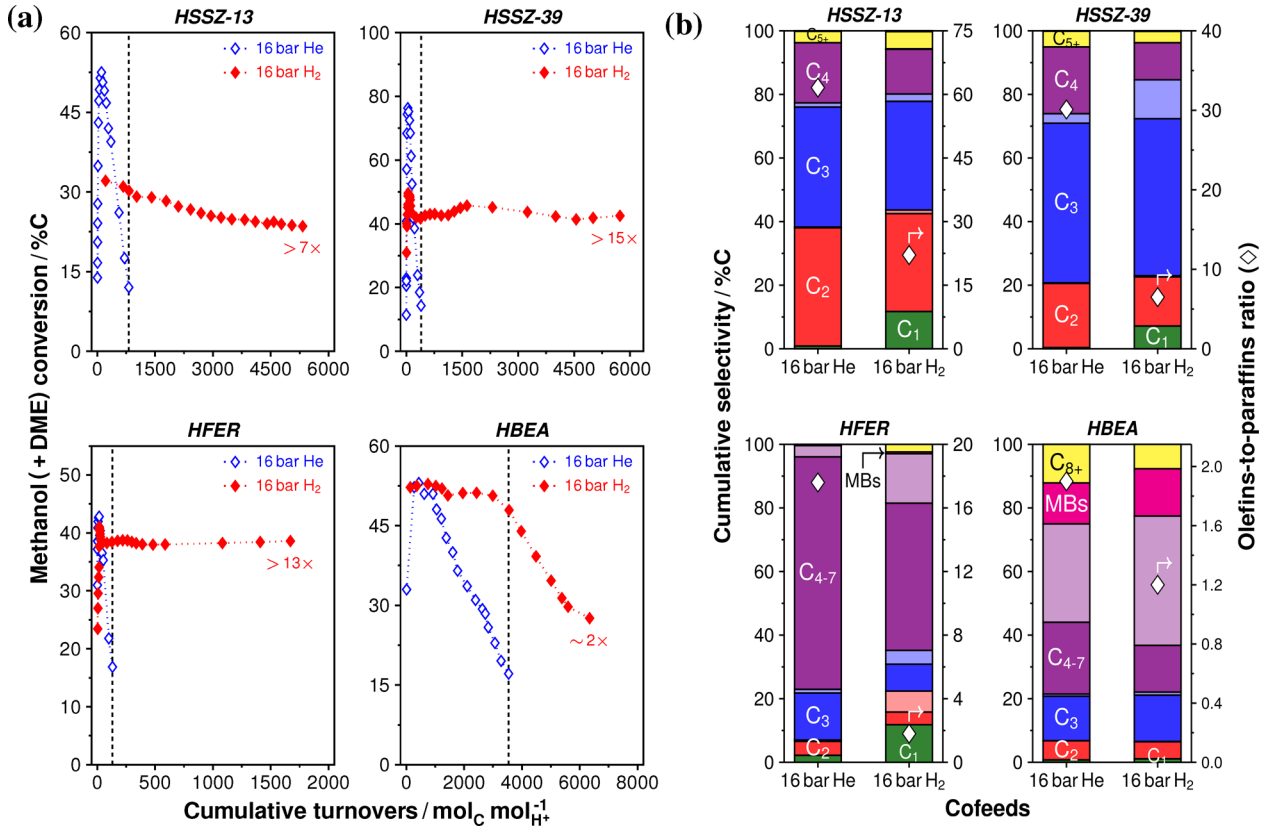

Figure 1. (a): Methanol conversion profiles versus cumulative turnovers; (b): Cumulative selectivity (left ordinate) and the overall olefins-to-paraffins ratio (right ordinate) in the effluent stream observed during methanol feeds with and without H_2 cofeeds over HSSZ-13, HSSZ-39, HFER, and HBEA. Reaction conditions: 623 K; 0.005 bar CH_3OH, 16 bar He or H_2 cofeed, 350 [HSSZ-13]; 114 [HSSZ-39]; 61 [HFER]; 89 [HBEA] mol_C $(mol_{H^+} \cdot ks)^{-1}$. (a) The vertical dashed lines denote the cumulative turnover capacity of the particular zeolite for methanol conversion with 16 bar He cofeed, which is used to calculate the relative lifetime improvement factors with 16 bar H_2 cofeeds (listed at the end of the red curves). (b) The dark- and light-shaded bars represent the olefinic and paraffinic forms, respectively, of the respective carbon group listed in the dark bars; "MBs" represents methyl-substituted benzenes.

Methanol Conversion with H_2 or He Cofeeds. Methanol (CHROMASOLV; Honeywell) was fed using a 100 mL stainless-steel syringe (Harvard Apparatus) and PHD ULTRA XF syringe pump (Harvard Apparatus) to heated lines and carried by the gas stream. The diluent [H_2 (99.9999%, Matheson)] and internal standard [N_2 (99.999%, Matheson)] flows were metered using mass flow controllers (Brooks). H_2 was substituted with He (99.9999%, Matheson) as the diluent in the control experiments. Product selectivities and methanol conversion (calculated based on the total amount of methanol/dimethyl ether (DME)-derived carbon atoms observed in the effluent hydrocarbons) profiles were measured during reactions of methanol (0.005 bar) with high-pressure (16 bar) H_2 or He cofeeds over packed beds comprised of HSSZ-13, HSSZ-39, HFER, and HBEA at 623 K and space velocities that resulted in subcomplete methanol conversion.

Ethene, Propene, and 1,3-Butadiene Hydrogenation with H_2. Ethene (0.1% in balance He, Primary Standard, Matheson), propene (0.1% in balance Ar, Certified Standard, Gasco), 1,3-butadiene (0.05% in balance He, Certified Standard, Praxair), H_2 (99.9999%, Matheson), and Ar (99.9999%, Matheson; used as the internal standard) flows were metered using mass flow controllers (Brooks 5850E). The steady-state hydrogenation rates were measured by adjusting the reactant flow rates to obtain the desired partial pressures of the respective reagents (0.0001−0.001 bar for the hydrocarbons and 1−16 bar for H_2) and space velocities that resulted in differential conditions (<5% conversion). The apparent enthalpic and entropic barriers were estimated from hydrogenation rate constants measured between 623 and 748 K.

RESULTS

Effects of H_2 Cofeeds on MTH Catalysis. As shown in Figure 1a, MTH lifetime, as assessed by cumulative turnovers, defined as the total amount of methanol/DME-derived carbon atoms observed in the effluent hydrocarbons normalized by the total acid sites in the catalyst bed,[28] attained until the final methanol conversion drops below 15%C, of HSSZ-13, HSSZ-39, HFER, and HBEA is considerably enhanced (~2× to >15×) with high-pressure (16 bar) H_2 cofeeds relative to the case of He cofeeds at equivalent concentrations under subcomplete methanol conversion conditions. These observations are in line with the results reported by Arora et al.[23] and Zhao et al.[29] during methanol conversion over HSAPO-34 and demonstrate the general utility of the proposed strategy of cofeeding high-pressure H_2 to markedly mitigate catalyst deactivation and prolong catalyst lifetimes during MTH over zeolites. Furthermore, as depicted in Figure 1b, these improvements in catalyst lifetime are observed without any impact on the carbon backbone of the effluent hydrocarbons characteristic of the particular zeolite topology. The maximum methanol conversion levels decrease with H_2 cofeeds relative to the case of He cofeeds over all zeolites. This is likely related to the increase in the

DOI: 10.1021/acscatal.9b00969
ACS Catal. 2019, 9, 6407−6414

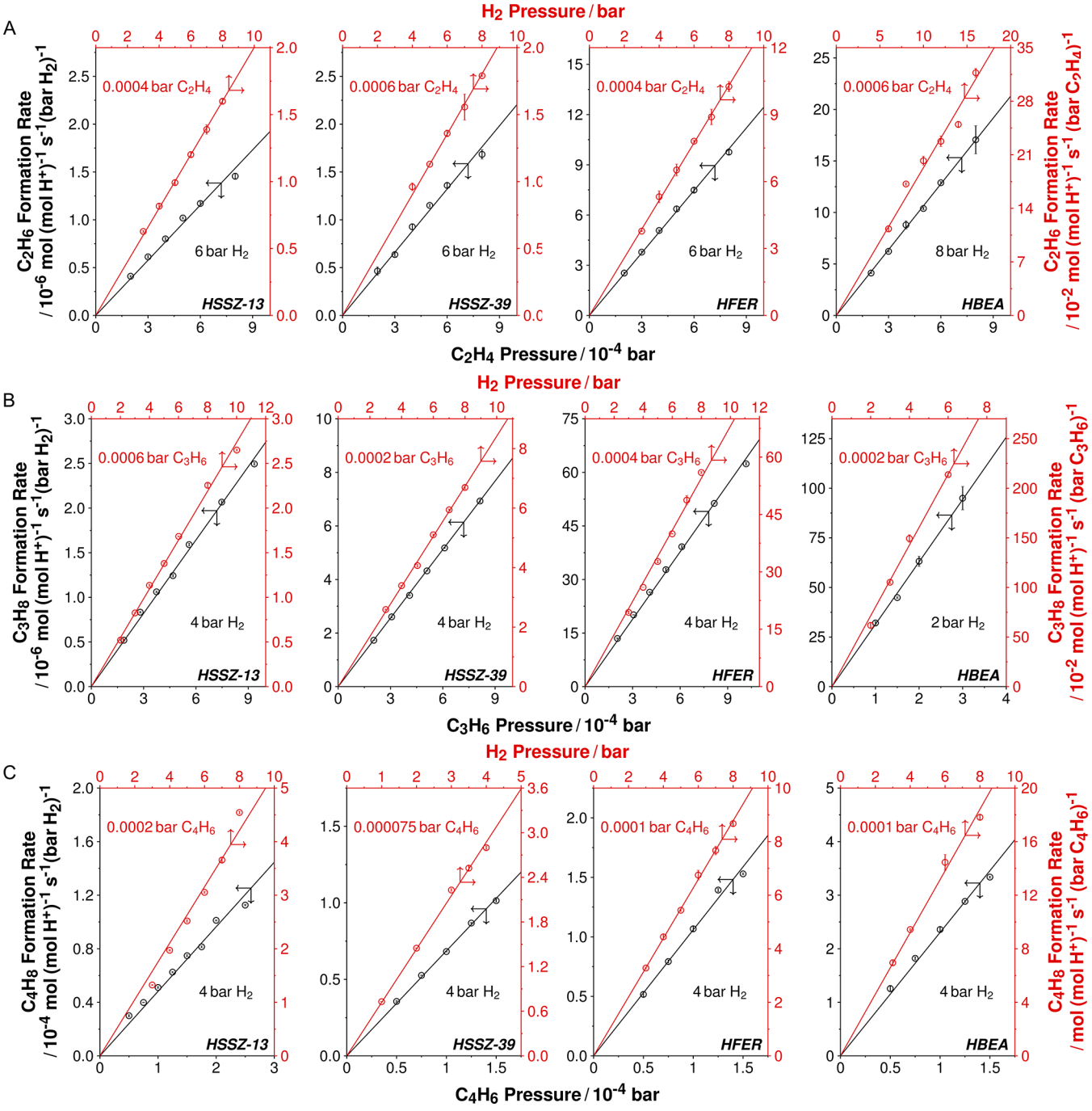

Figure 2. Dependencies of the formation rates of ethane, propane, and butenes on partial pressures of the hydrocarbon (bottom-left axes) and H_2 (top-right axes) during reactions of ethene (a), propene (b), and 1,3-butadiene (c) with H_2 over HSSZ-13, HSSZ-39, HFER, and HBEA at 673 K. The quantities listed along each line indicate the partial pressure of either the hydrocarbon or H_2 held constant while varying the partial pressure of the other reagent during the kinetic measurements. The vertical bars on each data point represent the standard-error associated with each measurement. The solid lines represent a linear fit to the experimental data.

production of paraffins with H_2 cofeeds since paraffins can be considered as terminal products under MTH conditions.[30]

The increase in paraffins production with H_2 cofeeds causes a decrement in the overall olefins-to-paraffins ratio, defined as the ratio of cumulative turnovers attained toward C_{2+} olefins and cumulative turnovers attained toward C_{2+} paraffins in the effluent over the catalyst lifetime, relative to the case of cofeeding He (Figure 1b). This decrement primarily arises from the enhanced production of C_2−C_4 paraffins over all zeolites, except in the case of HSSZ-39 where it is specifically a result of the higher formation of propane. Further, the magnitude of the decrement depends on the specific zeolite topology (~2.8× over HSSZ-13, ~4.6× over HSSZ-39, ~9.8× over HFER, and ~1.6× over HBEA).

We postulate that the observed effects of lifetime improvement and topology-dependent differences in the paraffin make of the MTH effluent with H_2 cofeeds can be mechanistically related to the relative reactivity of ethene, propene, and 1,3-butadiene with H_2 among the different zeolites. We evidence this by obtaining the rate constants for hydrogenation of the

DOI: 10.1021/acscatal.9b00969
ACS Catal. 2019, 9, 6407−6414

aforementioned species in independent kinetic studies, as detailed in the next section.

Kinetic Studies of Ethene, Propene, and 1,3-Butadiene Hydrogenation with H_2. Reactions of ethene, propene, and 1,3-butadiene (0.0001−0.001 bar) with high-pressure H_2 (1−16 bar) while maintaining high H_2-to-hydrocarbon ratios (>3000 in the case of ethene and propene and >12 000 in the case of 1,3-butadiene) at temperatures relevant for MTH catalysis (623−748 K) and differential conversions (<5%C) resulted in high selectivity of the first hydrogenated analogs—ethane (>99%C), propane (>80%C; balance CH_4 and C_2H_4 likely resulting from cracking of C_3H_8 or C_3H_6 oligomers), and a mix of butene isomers (>80%C; balance C_2H_4 and C_3H_6 likely resulting from cracking of C_4H_8 or C_4H_8 oligomers)—of the respective hydrocarbon reactant. The measured hydrogenation rates were stable with time-on-stream and depended weakly on the space velocity of the hydrocarbon reactant (Figure S3) indicating that the rate measurements were not affected by deactivation and secondary reactions or inhibition by products. Further, using the Weisz-Prater criterion[31] and measuring hydrogenation rates on a HFER sample with a different Si/Al ratio (= 27.5) than the one presented here (Si/Al = 10), it was verified that the measured rates are not corrupted by internal diffusion limitations and reflect solely the propensity of zeolitic protons confined in varying topological environments to catalyze the hydrogenation reactions under study (Table S2 and Figure S5).

Figure 2 shows that the measured formation rates of ethane, propane, and butene isomers normalized by the total Brønsted acid sites (H^+) in the catalyst bed are linearly dependent on the partial pressures of both the hydrocarbon [R = ethene (e), propene (p), and 1,3-butadiene (b)] and H_2 reactants and can be described by the rate expression shown in eq 1.

$$\frac{r_{RH_2}}{[H^+]} = k^R_{H_2} P_R P_{H_2} \quad (1)$$

The second-order rate constants ($k^R_{H_2}$), calculated as the slope of the linear fit to the observed rate measurements, of hydrogenation of ethene, propene, and 1,3-butadiene over the four zeolites considered in this study are tabulated in Table 2.

Table 2. Measured Second-Order Rate Constants [mol (mol H^+)$^{-1}$ s^{-1} (bar R)$^{-1}$ (bar H_2)$^{-1}$] of Hydrogenation of Hydrocarbons [R = Ethene (C_2H_4), Propene (C_3H_6), and 1,3-Butadiene (C_4H_6)] with H_2 over Acidic Zeolites at 673 K and their 95% Confidence Intervals

zeolite	$k^{C_2H_4}_{H_2}$	$k^{C_3H_6}_{H_2}$	$k^{C_4H_6}_{H_2}$
HSSZ-13	$0.0019 \pm 3 \times 10^{-5}$	$0.0027 \pm 3 \times 10^{-5}$	0.50 ± 0.01
HSSZ-39	$0.0022 \pm 3 \times 10^{-5}$	$0.0084 \pm 4 \times 10^{-5}$	0.70 ± 0.01
HFER	$0.013 \pm 9 \times 10^{-5}$	$0.066 \pm 7 \times 10^{-4}$	1.1 ± 0.01
HBEA	$0.020 \pm 3 \times 10^{-4}$	0.33 ± 0.006	2.3 ± 0.04

The observed rate expression for hydrogenation of hydrocarbon reactants over zeolites (eq 1) can be realized by a set of elementary steps shown in Scheme 1 under the following assumptions: (i) the fourth step involving the reaction between the surface intermediate derived from the hydrocarbon reactant (RH^+) and intrazeolite H_2 species (H_2 (z)) is rate-limiting, (ii) all other steps involving the adsorption/desorption of the reactants and products into and out of the zeolite channels are quasi-equilibrated, and (iii) Brønsted acid sites (H^+) are the dominant surface species. The observed rate dependencies are consistent with and the proposed set of elementary steps follow those reported by Gounder and Iglesia[32] for hydrogenation of propene on acidic zeolites.

Scheme 1. Elementary Steps Proposed for Hydrogenation of Hydrocarbons [R = Ethene (e), Propene (p), and 1,3-Butadiene (b)] with H_2 over Brønsted Acid (H^+) Zeolites[a]

R (g)	$\overset{k_1}{\underset{k_{-1}}{\rightleftharpoons}}$	R (z)	K_1
H_2 (g)	$\overset{k_2}{\underset{k_{-2}}{\rightleftharpoons}}$	H_2 (z)	K_2
R (z) + H^+	$\overset{k_3}{\underset{k_{-3}}{\rightleftharpoons}}$	RH^+	K_3
RH^+ + H_2 (z)	$\xrightarrow{\boldsymbol{k_4}}$	**RH_2 (z) + H^+**	$\boldsymbol{k_4}$
RH_2 (z)	$\overset{k_5}{\underset{k_{-5}}{\rightleftharpoons}}$	RH_2 (g)	K_5
R (g) + H_2 (g)	$\xrightarrow{k^R_{H_2}}$	RH_2 (g)	

$$r_{RH_2} = k_4 [RH^+][H_2(z)]$$

$$\frac{r_{RH_2}}{[H^+]} = \underbrace{k_4 K_3 K_2 K_1}_{k^R_{H_2}} P_R P_{H_2}$$

[a]The step highlighted in bold is considered as rate-limiting. The notations g and z in the parentheses denote the gas phase and intrazeolite phase, respectively.

The temperature dependence of the measured hydrogenation rate constants at fixed partial pressures of R and H_2 is presented in Figure 3 and can be described by the Arrhenius equation

$$\ln(k^R_{H_2}) = \ln A - \frac{E_a}{RT} \quad (2)$$

where A and E_a reflect the pre-exponential factors and the apparent enthalpic barriers, respectively, for the hydrogenation reactions. The pre-exponential factors in eq 2 can be used to calculate the apparent entropic barriers (ΔS_a) after accounting for the number of C−H bonds (n_b) in the first hydrogenated analogs of the hydrocarbon reactants (6, 8, and 8 for ethene, propene, and 1,3-butadiene, respectively) using eq 3, which follows the formalism reported by Gounder and Iglesia.[32,33] Under the observed kinetic regime characterized by first-order dependencies on both hydrocarbon and H_2 pressures, the measured apparent enthalpic (or entropic) barriers reflect the enthalpy (or entropy) difference between the hydrogenation transition state (TS) in the intrazeolite phase, and the gas-phase reactants (R and H_2) and the bare H^+ (eqs 4 and 6). Separately, considering the expression of the hydrogenation rate constant ($k^R_{H_2} = k_4 K_3 K_2 K_1$) deduced from the elementary steps proposed in Scheme 1, the apparent enthalpic (or entropic) barriers can also be interpreted as a combination of two components − (i) enthalpic gains (or entropic losses) resulting from adsorption of gas-phase reactants (R and H_2) into the confining voids of a zeolite, represented by ΔH_{ads} (or ΔS_{ads}) which arises from a

DOI: 10.1021/acscatal.9b00969
ACS Catal. 2019, 9, 6407−6414

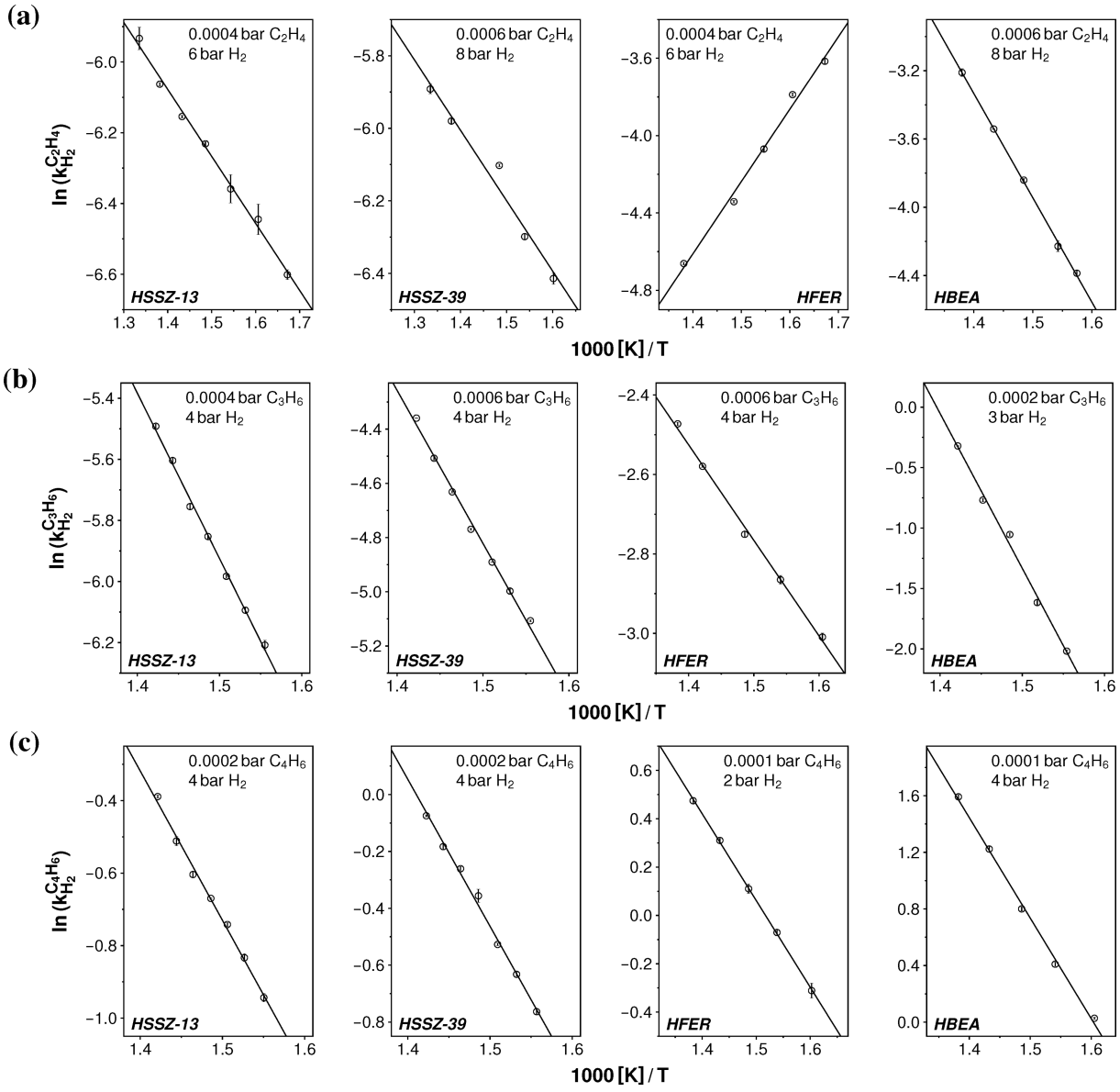

Figure 3. Temperature dependence of the measured second-order hydrogenation rate constants of ethene (a), propene (b), and 1,3-butadiene (c) hydrogenation with H_2 over HSSZ-13, HSSZ-39, HFER, and HBEA at 623−748 K. The pressures listed in each panel represent the partial pressures of the hydrocarbon reactant and H_2 that were held constant while varying the temperature. The vertical bars on each data point represent the standard-error associated with each measurement. The solid lines represent a linear fit to the experimental data.

Table 3. Apparent Enthalpic (E_a; [kJ mol^{-1}]) and Entropic (ΔS_a; [J mol^{-1} K^{-1}]) Barriers for Hydrogenation of Ethene, Propene, and 1,3-Butadiene over Acid Zeolites and their 95% Confidence Intervals

	ethene		propene		1,3-butadiene	
zeolite	E_a	ΔS_a	E_a	ΔS_a	E_a	ΔS_a
HSSZ-13	16 ± 1	−295 ± 1	45 ± 1	−251 ± 2	34 ± 1	−224 ± 2
HSSZ-39	16 ± 2	−294 ± 2	46 ± 1	−239 ± 2	43 ± 2	−208 ± 2
HFER	−31 ± 2	−348 ± 3	20 ± 1	−262 ± 1	30 ± 1	−224 ± 1
HBEA	51 ± 1	−223 ± 1	106 ± 5	−120 ± 8	59 ± 2	−174 ± 3

combination of K_1, K_2, and K_3; and (ii) enthalpic losses (or entropic gains) originating from reaction of the adsorbed intermediates to form the relevant transition state that transforms to the gas-phase product, represented by ΔH_{int} (or ΔS_{int}) which arises from k_4 (eqs 5 and 7). Accordingly, positive or negative values of the apparent enthalpic (or entropic) barriers reflect compensation between these enthalpic (or entropic) gains or losses during a certain reaction over a particular zeolite.[34−36] Specifically, a positive value of the apparent enthalpic barrier reflects a scenario when $\Delta H_{int} > \Delta H_{ads}$, and a negative value can be realized when $\Delta H_{int} < \Delta H_{ads}$. The experimentally measured values of these barriers for hydrogenation reactions of ethene, propene, and 1,3-butadiene over all zeolite samples used in the study are listed in Table 3. We

DOI: 10.1021/acscatal.9b00969
ACS Catal. 2019, 9, 6407−6414

note that the distinct topological features of the acidic zeolites can affect the measured enthalpic (or entropic) barriers by influencing ΔH_{ads} (or ΔS_{ads}) and ΔH_{int} (or ΔS_{int}); therefore, any interpretation of the observed differences based on their topology would require evaluation of both these components under reaction conditions.

$$\Delta S_a = R\left[\ln\left(\frac{A}{n_b}\right) - \ln\left(\frac{k_B T}{h}\right)\right] \quad (3)$$

$$E_a = E_{TS} - E_{R(g)} - E_{H_2(g)} - E_{H^+} \quad (4)$$

$$E_a = \Delta H_{int} - \Delta H_{ads} \quad (5)$$

$$\Delta S_a = \Delta S_{TS} - \Delta S_{R(g)} - \Delta S_{H_2(g)} - \Delta S_{H^+} \quad (6)$$

$$\Delta S_a = \Delta S_{int} - \Delta S_{ads} \quad (7)$$

As shown in Table 2, the measured hydrogenation rate constants of 1,3-butadiene are at least 1 order-of-magnitude (~7× to ~320×) higher than the corresponding values for ethene and propene over all zeolites used in the study. This difference is indicative of the high reactivity of 1,3-butadiene with H_2 which consequently results in interception of its further transformation to aromatics and polycyclics, and provides a mechanistic basis for the observed enhancements in catalyst lifetime during MTH with H_2 cofeeds. We propound that the weak hydrogenation ability of Brønsted acid sites in zeolites relative to metal-based hydrogenation catalyst formulations, and the higher degree of unsaturation in 1,3-butadiene than in ethene and propene likely results in the observed higher reactivity of 1,3-butadiene with H_2 compared to ethene and propene.

Further, we analyze the topology-dependent decrements in the olefins-to-paraffins ratios of effluent with H_2 cofeeds in context of the measured hydrogenation rate constants of ethene and propene that are observed to be dictated by the zeolite topology (Table 2). The low (~2.8×) decrement in the olefins-to-paraffins ratio or correspondingly, the predominance of C_2−C_4 olefins over their paraffinic counterparts during MTH with H_2 cofeeds over HSSZ-13 compared to other zeolites can be explained by the lowest values of the hydrogenation rate constants of ethene [0.0019 versus 0.013−0.020 mol (mol H^+)$^{-1}$ s^{-1} (bar C_2H_4)$^{-1}$ (bar H_2)$^{-1}$] and propene [0.0027 versus 0.0084−0.33 mol (mol H^+)$^{-1}$ s^{-1} (bar C_3H_6)$^{-1}$ (bar H_2)$^{-1}$] over HSSZ-13 among the zeolites used in the study. In the case of HSSZ-39 compared to HSSZ-13, the higher selectivity of propane in the MTH effluent with H_2 cofeeds can be explicated by the higher value [0.0084 versus 0.0027 mol (mol H^+)$^{-1}$ s^{-1} (bar C_2H_6)$^{-1}$ (bar H_2)$^{-1}$] of the measured rate constant of propene hydrogenation relative to HSSZ-13, while the insignificant increase in ethane formation can be considered a result of its low activity [0.0022 mol (mol H^+)$^{-1}$ s^{-1} (bar C_3H_4)$^{-1}$ (bar H_2)$^{-1}$] for ethene hydrogenation which is similar to HSSZ-13. The measured rate constants of hydrogenation of ethene [0.013 mol (mol H^+)$^{-1}$ s^{-1} (bar C_2H_4)$^{-1}$ (bar H_2)$^{-1}$] and propene [0.066 mol (mol H^+)$^{-1}$ s^{-1} (bar C_3H_6)$^{-1}$ (bar H_2)$^{-1}$] are both observed to be significantly higher on HFER relative to both HSSZ-13 and HSSZ-39, and expound the highest decrement (~9.8×) in the olefins-to-paraffins ratio during MTH with H_2 cofeeds. HBEA, however, deviates from the trend and although the hydrogenation rate constants of ethene, propene, and 1,3-butadiene are highest among the zeolites considered, the effects on lifetime (~2× increment) and olefins-to-paraffins ratio (~1.6× decrement) with H_2 cofeeds are less significant compared to other zeolites (Figure 1). This is likely a consequence of the relatively high lifetime (~3500 versus ~130−800 mol_C $mol_{H^+}^{-1}$) and low olefins-to-paraffins ratio (~1.9 versus ~17.6−61.6) observed in the baseline MTH case with He cofeeds over HBEA compared to other zeolites.

CONCLUSIONS

The effectiveness of high-pressure H_2 cofeeds to enhance catalyst lifetime during MTH catalysis is demonstrated for four different zeolites (HSSZ-13, HSSZ-39, HFER, and HBEA) with varying topologies (CHA, AEI, FER, and BEA) validating the general utility of the proposed strategy. This effect of lifetime improvement with H_2 cofeeds can be mechanistically related to the higher proclivity of 1,3-butadiene to undergo hydrogenation with H_2, relative to ethene and propene, which intercepts its further transformation and likely leads to suppressed production of deactivation-inducing polycyclics during methanol conversion. The topology-dependent variations in the paraffin make of the effluent hydrocarbons during MTH with H_2 cofeeds over different zeolites can be interpreted based on the varying catalytic behavior of protons toward hydrogenation of ethene and propene, wherein a higher predisposition for these reactions is observed to correspond to lower olefins-to-paraffins ratios or higher paraffins production during MTH with H_2 cofeeds.

ASSOCIATED CONTENT

Supporting Information

The Supporting Information is available free of charge on the ACS Publications website at DOI: 10.1021/acscatal.9b00969.

Catalyst characterization (NH_3-TPD, pyridine IR, and XRD) results; and consideration of stability, and effects of space-velocity and internal diffusion limitations on the rate measurements. (PDF)

AUTHOR INFORMATION

Corresponding Author

*E-mail: abhan@umn.edu.

ORCID

Aditya Bhan: 0000-0002-6069-7626

Author Contributions

‡S.S.A. and Z.S. contributed equally to the work.

Notes

The authors declare no competing financial interest.

ACKNOWLEDGMENTS

The authors thank (i) Dow through the University Partnership Initiative and the National Science Foundation (CBET 1701534) for financial support, (ii) Dr. Andrzej Malek, Dr. Davy L. S. Nieskens, and Dr. Joseph DeWilde from Dow for helpful technical discussions, (iii) Dr. Nicholas Seaton from the University of Minnesota Characterization Facility, which receives partial support from the National Science Foundation through the Materials Research Science and Engineering Centers program, for providing the EDS data, and (iv) Mr. Xinyu Li from University of Minnesota for providing the X-ray diffractograms for all zeolite samples and pyridine IR spectra for the HBEA sample.

DOI: 10.1021/acscatal.9b00969
ACS Catal. 2019, 9, 6407−6414

REFERENCES

(1) Baerlocher, C.; McCusker, L. B.; Olson, D. *Atlas of zeolite framework types*; Elsevier: Amsterdam, 2007.

(2) Bhawe, Y.; Moliner-Marin, M.; Lunn, J. D.; Liu, Y.; Malek, A.; Davis, M. Effect of Cage Size on the Selective Conversion of Methanol to Light Olefins. *ACS Catal.* **2012**, *2*, 2490−2495.

(3) Martín, N.; Li, Z.; Martínez-Triguero, J.; Yu, J.; Moliner, M.; Corma, A. Nanocrystalline SSZ-39 zeolite as an efficient catalyst for the methanol-to-olefin (MTO) process. *Chem. Commun.* **2016**, *52*, 6072−6075.

(4) Dusselier, M.; Davis, M. E. Small-Pore Zeolites: Synthesis and Catalysis. *Chem. Rev.* **2018**, *118*, 5265−5329.

(5) Haw, J. F.; Song, W.; Marcus, D. M.; Nicholas, J. B. The mechanism of methanol to hydrocarbon catalysis. *Acc. Chem. Res.* **2003**, *36*, 317−326.

(6) Svelle, S.; Olsbye, U.; Joensen, F.; Bjørgen, M. Conversion of Methanol to Alkenes over Medium- and Large-Pore Acidic Zeolites: Steric Manipulation of the Reaction Intermediates Governs the Ethene/Propene Product Selectivity. *J. Phys. Chem. C* **2007**, *111*, 17981−17984.

(7) Olsbye, U.; Svelle, S.; Bjørgen, M.; Beato, P.; Janssens, T. V. W.; Joensen, F.; Bordiga, S.; Lillerud, K. P. Conversion of Methanol to Hydrocarbons: How Zeolite Cavity and Pore Size Controls Product Selectivity. *Angew. Chem. Int. Ed.* **2012**, *51*, 5810−5831.

(8) Olsbye, U.; Bjørgen, M.; Svelle, S.; Lillerud, K.-P.; Kolboe, S. Mechanistic insight into the methanol-to-hydrocarbons reaction. *Catal. Today* **2005**, *106*, 108−111.

(9) Svelle, S.; Joensen, F.; Nerlov, J.; Olsbye, U.; Lillerud, K.-P.; Kolboe, S.; Bjørgen, M. Conversion of methanol into hydrocarbons over zeolite H-ZSM-5: ethene formation is mechanistically separated from the formation of higher alkenes. *J. Am. Chem. Soc.* **2006**, *128*, 14770−1.

(10) Bjørgen, M.; Svelle, S.; Joensen, F.; Nerlov, J.; Kolboe, S.; Bonino, F.; Palumbo, L.; Bordiga, S.; Olsbye, U. Conversion of methanol to hydrocarbons over zeolite H-ZSM-5: On the origin of the olefinic species. *J. Catal.* **2007**, *249*, 195−207.

(11) Bjørgen, M.; Joensen, F.; Lillerud, K.-P.; Olsbye, U.; Svelle, S. The mechanisms of ethene and propene formation from methanol over high silica H-ZSM-5 and H-beta. *Catal. Today* **2009**, *142*, 90−97.

(12) Ilias, S.; Bhan, A. Mechanism of the Catalytic Conversion of Methanol to Hydrocarbons. *ACS Catal.* **2013**, *3*, 18−31.

(13) Schulz, H. Coking" of zeolites during methanol conversion: Basic reactions of the MTO-, MTP- and MTG processes. *Catal. Today* **2010**, *154*, 183−194.

(14) Olsbye, U.; Svelle, S.; Lillerud, K. P.; Wei, Z. H.; Chen, Y. Y.; Li, J. F.; Wang, J. G.; Fan, W. B. The formation and degradation of active species during methanol conversion over protonated zeotype catalysts. *Chem. Soc. Rev.* **2015**, *44*, 7155−7176.

(15) Müller, S.; Liu, Y.; Vishnuvarthan, M.; Sun, X.; van Veen, A. C.; Haller, G. L.; Sanchez-Sanchez, M.; Lercher, J. A. Coke formation and deactivation pathways on H-ZSM-5 in the conversion of methanol to olefins. *J. Catal.* **2015**, *325*, 48−59.

(16) Müller, S.; Liu, Y.; Kirchberger, F. M.; Tonigold, M.; Sanchez-Sanchez, M.; Lercher, J. A. Hydrogen Transfer Pathways during Zeolite Catalyzed Methanol Conversion to Hydrocarbons. *J. Am. Chem. Soc.* **2016**, *138*, 15994−16003.

(17) Hwang, A.; Kumar, M.; Rimer, J. D.; Bhan, A. Implications of methanol disproportionation on catalyst lifetime for methanol-to-olefins conversion by HSSZ-13. *J. Catal.* **2017**, *346*, 154−160.

(18) Martinez-Espin, J. S.; De Wispelaere, K.; Westgård Erichsen, M.; Svelle, S.; Janssens, T. V.; Van Speybroeck, V.; Beato, P.; Olsbye, U. Benzene co-reaction with methanol and dimethyl ether over zeolite and zeotype catalysts: Evidence of parallel reaction paths to toluene and diphenylmethane. *J. Catal.* **2017**, *349*, 136−148.

(19) Martinez-Espin, J. S.; Mortén, M.; Janssens, T. V. W.; Svelle, S.; Beato, P.; Olsbye, U. New insights into catalyst deactivation and product distribution of zeolites in the methanol-to-hydrocarbons (MTH) reaction with methanol and dimethyl ether feeds. *Catal. Sci. Technol.* **2017**, *7*, 2700−2716.

(20) Martinez-Espin, J. S.; De Wispelaere, K.; Janssens, T. V. W.; Svelle, S.; Lillerud, K. P.; Beato, P.; Van Speybroeck, V.; Olsbye, U. Hydrogen Transfer versus Methylation: On the Genesis of Aromatics Formation in the Methanol-To-Hydrocarbons Reaction over H-ZSM-5. *ACS Catal.* **2017**, *7*, 5773−5780.

(21) Arora, S. S.; Bhan, A. The critical role of methanol pressure in controlling its transfer dehydrogenation and the corresponding effect on propylene-to-ethylene ratio during methanol-to-hydrocarbons catalysis on H-ZSM-5. *J. Catal.* **2017**, *356*, 300−306.

(22) Liu, Y.; Kirchberger, F. M.; Müller, S.; Eder, M.; Tonigold, M.; Sanchez-Sanchez, M.; Lercher, J. A. Critical role of formaldehyde during methanol conversion to hydrocarbons. *Nat. Commun.* **2019**, *10*, 1462.

(23) Arora, S. S.; Nieskens, D. L. S.; Malek, A.; Bhan, A. Lifetime improvement in methanol-to-olefins catalysis over chabazite materials by high-pressure H_2 co-feeds. *Nat. Catal.* **2018**, *1*, 666−672.

(24) Adams, D. R.; Bhatnagar, S. P. The Prins Reaction. *Synthesis* **1977**, *1977*, 661−672.

(25) Vasiliadou, E. S.; Gould, N. S.; Lobo, R. F. Zeolite-Catalyzed Formaldehyde-Propylene Prins Condensation. *ChemCatChem* **2017**, *9*, 4417−4425.

(26) Harris, J. W.; Cordon, M. J.; Di Iorio, J. R.; Vega-Vila, J. C.; Ribeiro, F. H.; Gounder, R. Titration and quantification of open and closed Lewis acid sites in Sn-Beta zeolites that catalyze glucose isomerization. *J. Catal.* **2016**, *335*, 141−154.

(27) Selli, E.; Forni, L. Comparison between the surface acidity of solid catalysts determined by TPD and FTIR analysis of pre-adsorbed pyridine. *Microporous Mesoporous Mater.* **1999**, *31*, 129−140.

(28) Hwang, A.; Prieto-Centurion, D.; Bhan, A. Isotopic tracer studies of methanol-to-olefins conversion over HSAPO-34: The role of the olefins-based catalytic cycle. *J. Catal.* **2016**, *337*, 52−56.

(29) Zhao, X.; Li, J.; Tian, P.; Wang, L.; Li, X.; Lin, S.; Guo, X.; Liu, Z. Achieving a Superlong Lifetime in the Zeolite-Catalyzed MTO Reaction under High Pressure: Synergistic Effect of Hydrogen and Water. *ACS Catal.* **2019**, *9*, 3017−3025.

(30) Ilias, S.; Khare, R.; Malek, A.; Bhan, A. A descriptor for the relative propagation of the aromatic- and olefin-based cycles in methanol-to-hydrocarbons conversion on H-ZSM-5. *J. Catal.* **2013**, *303*, 135−140.

(31) Weisz, P.; Prater, C. Interpretation of Measurements in Experimental Catalysis. *Adv. Catal.* **1954**, *6*, 143−196.

(32) Gounder, R.; Iglesia, E. Catalytic hydrogenation of alkenes on acidic zeolites: Mechanistic connections to monomolecular alkane dehydrogenation reactions. *J. Catal.* **2011**, *277*, 36−45.

(33) Gounder, R.; Iglesia, E. Catalytic Consequences of Spatial Constraints and Acid Site Location for Monomolecular Alkane Activation on Zeolites. *J. Am. Chem. Soc.* **2009**, *131*, 1958−1971.

(34) Bhan, A.; Gounder, R.; Macht, J.; Iglesia, E. Entropy considerations in monomolecular cracking of alkanes on acidic zeolites. *J. Catal.* **2008**, *253*, 221−224.

(35) Gounder, R.; Iglesia, E. The Roles of Entropy and Enthalpy in Stabilizing Ion-Pairs at Transition States in Zeolite Acid Catalysis. *Acc. Chem. Res.* **2012**, *45*, 229−238.

(36) Sarazen, M. L.; Iglesia, E. Stability of bound species during alkene reactions on solid acids. *Proc. Natl. Acad. Sci.* **2017**, *114*, E3900−E3908.

DOI: 10.1021/acscatal.9b00969
ACS Catal. 2019, 9, 6407−6414